Terahertz photomixing using plasma resonances in double-graphene layer structures

V. Ryzhii, M. Ryzhii, V. Mitin, M. S. Shur, A. Satou et al.

Citation: J. Appl. Phys. **113**, 174506 (2013); doi: 10.1063/1.4804063
View online: http://dx.doi.org/10.1063/1.4804063
View Table of Contents: http://jap.aip.org/resource/1/JAPIAU/v113/i17
Published by the American Institute of Physics.

Terahertz photomixing using plasma resonances in double-graphene layer structures

V. Ryzhii,[1,a)] M. Ryzhii,[2] V. Mitin,[3] M. S. Shur,[4] A. Satou,[1] and T. Otsuji[1]
[1]*Research Institute for Electrical Communication, Tohoku University, Sendai 980-8577, Japan*
[2]*Computational Nanoelectronics Laboratory, University of Aizu, Aizu-Wakamatsu 965-8580, Japan*
[3]*Department of Electrical Engineering, University at Buffalo, Buffalo, New York 1460-1920, USA*
[4]*Department of Electrical, Electronics, and Systems Engineering and Physics, Applied Physics, and Astronomy, Rensselaer Polytechnic Institute, Troy, New York 12180, USA*

(Received 29 January 2013; accepted 22 April 2013; published online 7 May 2013)

We propose the concept of terahertz (THz) photomixing enabled by the interband electron transitions due to the absorption of modulated optical radiation in double-graphene layer (double-GL) structures and the resonant excitation of plasma oscillations. Using the developed double-GL photomixer (DG-PM) model, we describe its operation and calculate the device characteristics. The output power of the THz radiation exhibits sharp resonant peaks at the plasmonic resonant frequencies. The peak powers markedly exceed the output powers at relatively low frequencies. Due to relatively high quantum efficiency of optical absorption in GLs and short inter-GL transit time, the proposed DG-PM operating in the resonant plasma oscillation regime can surpass the photomixers based on the standard heterostructures. © *2013 AIP Publishing LLC*. [http://dx.doi.org/10.1063/1.4804063]

I. INTRODUCTION

The energy spectrum of graphene layers (GLs) enables the interband photogeneration of electrons and holes by electromagnetic radiation from the terahertz (THz) to ultraviolet range.[1–3] This provides an opportunity to use GL structures in active and passive optoelectronic devices. Long momentum relaxation times in GLs[4] promote the existence of different modes of weakly damped propagating and standing plasma waves (oscillations) in GL-structures, in particular, in the gated GLs at THz frequencies,[5–10] as well as plasmon-polaritons.[11,12] The variation of the gate voltage, V_0, in such structures with highly conducting gates tunes the plasma frequencies, which are proportional to $V_0^{1/4}$.[5,7] This voltage dependence is different from that in the gated structures with two-dimensional gas of the electrons with the standard (near parabolic) energy spectrum, in which the plasma frequency is proportional to $V_0^{1/2}$ (see, for instance, Ref. 13). The distinction of the voltage dependences in question is associated with the dependence of the "fictitious" mass of electrons and holes in GLs on the electron and hole densities and, hence, on the gate voltage. The gapless energy spectrum of GLs and the expected weak damping of different plasma waves in GLs opens up the prospects of creation of different THz plasma-wave GL-based devices, such as THz photomixers, surpassing those made of the standard heterostructures such as high-electron mobility transistors (see, for example, Refs. 13–21). In recently fabricated and analyzed double-GL structures,[22–25] the propagating and standing plasma waves can exhibit nontrivial properties. In particular, in the double-GL structures the waves, in which the electron and hole densities oscillate in the same phases, are similar to those in the gated structures and the linear plasma wave dispersion relation (the plasma frequency is approximately proportional to the wave number, $\omega_p \propto q$). This is because in these structures each GL plays the role of a highly conducting gate for the other GL.[26,27] The ac electric field in such syn-phase plasma modes is mainly located between GLs. In the double-GL and multiple-GL structures, other plasma modes exist, including the waves with the opposite phases of the electron and hole density variation with $\omega_p \propto q$ (Refs. 28 and 29) and the plasmon-polariton modes with rather complex spectrum.[30]

In this paper, we propose to use the double-GL structures irradiated by two coherent optical sources, i.e., lasers with the photon frequencies, Ω_1 and Ω_2, close to each other, so that the modulation frequency, ω, is equal to $\omega = \Omega_2 - \Omega_1$) or by ultra-short optical pulses for the generation of THz radiation (THz photomixing). The device operation is associated with the ac photocurrent between GLs at the difference frequency ω. The radiation induced photocurrent between GLs induces the ac terminal current, which feeds an antenna emitting the radiation with the frequency ω. As shown in the following, when ω approaches to the frequencies of the plasma oscillation modes (with the syn-phase variations of the electron and hole densities), the excitation of plasma oscillations in the double-GL structures occurs, and the ac inter-GL photocurrent can be resonantly large.

The spectrum of the plasma modes in the double-GL structures with limited length is determined by the quantization rule $\omega = \omega_n \propto q_n$. Here q_n is the wave numbers ($n = 0$, 1, 2,…). The latter are determined by the specifics of the boundary conditions.

In the double-GL structures with the inter-GL barrier made of hexagonal boron nitride (hBN),[23] the barrier height is large, so that the effective generation of the inter-GL photocurrent is possible only if the photon energies $\hbar\Omega_1$ and $\hbar\Omega_2$ are rather large (about several eV). However, as demonstrated recently,[25] in double-GL structures with a very thin

a)Electronic mail: v-ryzhii(at)riec.tohoku.ac.jp

tungsten disulphide (WS_2) between GLs (or some similar compounds), the barrier for electrons is relatively low (so that, depending on the values of the barrier height and the electron energy, the inter-GL current can be associated with both tunneling through the barrier and thermionic emission over the barrier). In such structures, the photoemission of electrons from one GL to another caused by the absorption of photons with $\hbar\Omega_1 \simeq \hbar\Omega_2 \sim 1$ eV can be effective. The possibility to vary the electron and hole densities in GLs by the applied bias voltage provides an opportunity to control the resonant plasma frequencies by this voltage.

To substantiate the concept of the double-GL photomixer (DGL-PM) under consideration, we develop a model for the pertinent device, calculate its characteristics, and evaluate the device performance. The resonant response of DGM-PMs, associated with the excitation of plasma oscillation, provides significant advantages over the THz photomixers based on the low-temperature-grown GaAs photoconductive switch,[31] p-i-n photodiodes,[32] and unitravelling-carrier photodiodes (UTC-PDs).[33,34] Relatively strong absorption in GLs and ultra-short transit time across the inter-GL barrier can result in the DGL-PM performance exceeding that of UTC-PDs even with the integrated plasma cavity.[35]

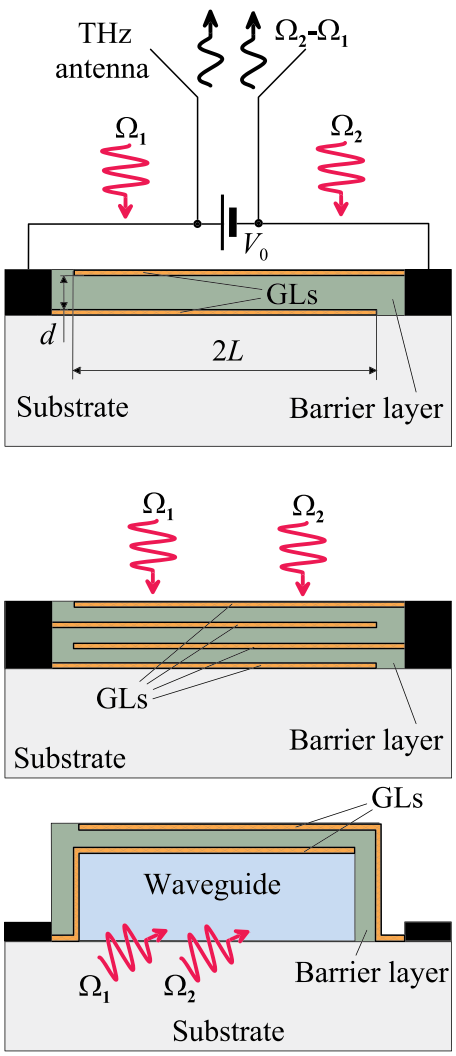

FIG. 1. Schematic view of the DG-PM with double-GL device (upper panel). Lower panels correspond to DG-PM structures with the system of multiple stacked double-GLs and to DG-PM integrated with an optical waveguide.

II. MODEL

We consider DG-PMs with the inter-GL barrier made of a material like WS_2, which forms a relatively low barrier for electrons (and rather high barrier for holes) or of a very thin layer with sufficient tunneling transparency for the photoexcited electrons. We focus on the device structures shown in Fig. 1 (upper panel). It is assumed that each GL is supplied with a side contact. The bias voltage, V_0, is applied between these contacts to induce the extra electrons in one GL (upper) and holes in another (lower), referred to as the n- and p-GLs, respectively. It is assumed that the intensity, I, of the incoming optical radiation comprises the ac component (the beating intensity) $\delta I \exp(-i\omega t)$. In the case of irradiation by two lasers with close frequencies, $\delta I \propto \sqrt{2I_1 I_2}$, where I_1 and I_2 are the intensities of radiation emitted by the lasers with the frequency $\Omega_1 = \Omega$ and $\Omega_2 = \Omega + \omega$, respectively.

The electrons photoexcited in the n-GL due to the interband transitions associated with the absorption of the incident photons can easily escape from this GL to another GL over the barrier if $\hbar\Omega/2 > \Delta_e = \Delta_C$ (see Fig. 2, upper panel), while the photoexcited electrons in the p-GL cannot leave it over the barrier until when $\hbar\Omega/2 > \Delta_h = \Delta_C + 2\mu$. Here, $\mu_+ = \mu_- \hbar v_W \sqrt{\kappa V_0/4ed} = \mu$ is the Fermi energy of electrons and holes, where $v_W \simeq 10^8$ cm/s is the characteristic velocity of electrons and holes in GLs, $\hbar$ is the reduced Planck constant, e is the electron charge, and κ and d are the dielectric constant and the inter-GL barrier layer thickness, respectively. At $\hbar\Omega/2 > \Delta_h, \Delta_e$, the electrons excited in both GLs can transfer to another GL, but the net inter-GL current caused by the photoexcited electrons is very small because the electron fluxes from the n-GL to the p-GL and back virtually compensate each other. If $\Delta_e < \hbar\Omega/2 < \Delta_h$, the

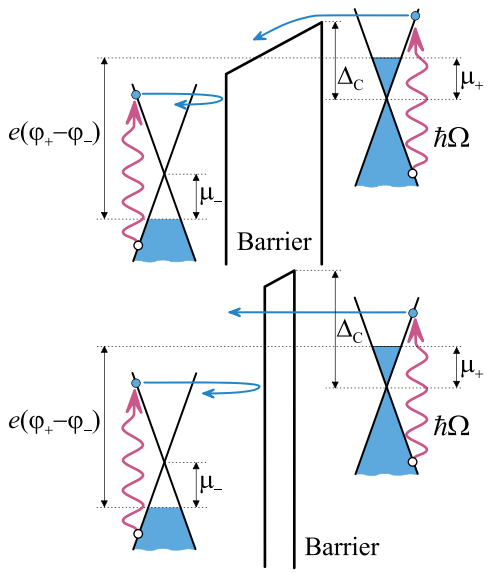

FIG. 2. Energy band diagram for the device under consideration with thermionic inter-GL current (upper panel) and with tunneling inter-GL current (lower panel) at bias voltage. Quantity $(\varphi_+ - \varphi_-)$ is the difference of local potentials in GLs, which under dc conditions is equal to V_0.

electron flux from n-GL to p-GL dominates, and the inter-GL photocurrent due to the photoelectrons passing over the barrier appears. In this case, only a weak component of the electron flux from the p-GL to the n-GL can exist only due to the inter-GL tunneling.

To avoid strong inter-GL dc current, the Fermi energy μ should not exceed the barrier height Δ_C. The above conditions correspond to the following relationship between the barrier height, the photon energy, and the bias voltage:

$$0 < \hbar\Omega - 2\Delta_C < 2\hbar\, v_W \sqrt{\frac{\kappa V_0}{ed}} < 2\Delta_C. \tag{1}$$

At the photon energy $\hbar\Omega$ smaller than the barrier height Δ_C, the inter-GL photocurrent is associated with the electron tunneling from the n-GL to p-GL, which prevails the tunneling from the p-GL to the n-GL due to lower effective barrier height in the former case (see Fig. 2, lower panel). In such a situation, the photocurrent can be moderate, but sufficient for the photomixing, particularly, if accompanied with the plasma oscillations excitation.

The consideration of the thermionic and tunneling mechanisms of DGL-PM operation can be combined by the introduction of the phenomenological parameter—the net probability of escape of the photoexcited electrons w_{esc}. Since the spacing, d, between GLs is rather small compared to the lateral size, $2L$, one can use the following formulas which relate the charge densities $e\Sigma_\pm$ (with $-\Sigma_+$ being virtually equal to the electron density in the upper, "electron," GL while Σ_- being close to the hole density in the lower, "hole," GL) and the electric potentials (Poisson equation in the gradual channel approximation):

$$\frac{4\pi e\Sigma_+}{\kappa} = -\frac{(\varphi_+ - \varphi_-)}{d}, \qquad \frac{4\pi e\Sigma_-}{\kappa} = \frac{(\varphi_+ - \varphi_-)}{d}. \tag{2}$$

The negative values of $e\Sigma_\pm$ correspond to the case when a GL is filled primarily with electrons, whereas the positive values correspond to the filling by holes.

In the framework of the DG-PM device model under consideration, we describe the dynamics of the electron-hole system perturbed by the modulated optical radiation using the linearized hydrodynamic equations (i.e., using the small signal analysis). These equations are adjusted for the features of the energy spectrum of GLs.[10] In the situation under consideration, the linearized continuity equations can be presented as

$$-i\omega\delta\Sigma_+ - \Sigma_0\frac{d\delta u_+}{dx} = \frac{\delta j}{e}, \tag{3}$$

$$-i\omega\delta\Sigma_- + \Sigma_0\frac{d\delta u_-}{dx} = -\frac{\delta j}{e}. \tag{4}$$

Here $e\delta\Sigma_\pm$ and $\delta u_\pm$ are the ac components of the GL charges and the average (hydrodynamic) velocities of electrons and holes along GLs, δj is the density of the inter-GL current, Σ_0 is the equilibrium density of electrons and holes in the pertinent GLs, and the axis x is directed along the GL plane. Considering the balance between the processes of the electron photoexcitation, the electron escape from one GL to another, and the electron relaxation in GLs, we obtain

$$\delta j = \frac{e\beta}{(1 + \tau_{esc}/\tau_{relax} - i\omega\tau_{esc})}\frac{[\exp(i\omega\tau_{tr}) - 1]}{i\omega\tau_{tr}}\frac{\delta I}{\hbar\Omega}. \tag{5}$$

Here, $\beta = \pi e^2/\hbar c \simeq 0.023$, c is the speed of light, τ_{esc} is the characteristic time of the photoexcited electron thermionic or tunneling escape from GL, $1/\tau_{relax} = 1/\tau_0 + 1/\tau_{cc} + 1/\tau_{rec}$, where τ_0, τ_{cc}, and τ_{rec} are the characteristic times of the optical phonon emission, inter-carrier collisions, and recombination, and τ_{tr} is the transit time across the barrier layer. The factor containing the value of the transit time τ_{tr} reflects the effect of finiteness of the transit time. Taking into account that in DG-PM the thickness of the barrier layer is rather small, even in the THz range of frequencies $\omega\tau_{tr} \ll 1$, hence, the factor in question can set to be equal to unity. Introducing the low frequency responsivity $R_{0,}$

$$R_0 = \frac{e\beta\, w_{esc}}{\hbar\Omega}, \tag{6}$$

the inter-GL ac current and the responsivity can be presented as

$$\delta j = \frac{R_0}{(1 - i\omega\tau_e)}\delta I, \qquad R = \frac{R_0}{(1 - i\omega\tau_e)}, \tag{7}$$

where $w_{esc} = (1 + \tau_{esc}/\tau_{relax})^{-1} = [1 + \tau_{esc}(\frac{1}{\tau_0} + \frac{1}{\tau_{cc}} + \frac{1}{\tau_{rec}})]^{-1}$ is the probability of the photoexcited electron escape from the n-GL to the p-GL and $\tau_e = \tau_{esc}\tau_{relax}/(\tau_{esc} + \tau_{relax}) = \tau_{relax}(1 - w_{esc})$ is the time, which characterizes the behavior of photoexcited electrons in GLs.

III. EXCITATION OF PLASMA OSCILLATIONS

The net ac inter-GL current is due to not only to the ac current induced by the photoexcited electrons passing from one GL to another, but also due to the displacement current. The latter is determined by the spatial distribution along GLs of the local ac potential difference $(\delta\varphi_+ - \delta\varphi_-)$. Generally, this distribution is essentially nonuniform stemmed from nonuniform spatial distributions of the ac components of the electron and hole densities. The uniformity in question can be particularly strong in the case of the excitation of plasma oscillations. Complementing Eqs. (2)–(4) with the linearized version of the hydrodynamic Euler equation governing the quantities $\delta u_\pm$, one can reduce the problem of finding the spatial distributions of the ac potential, $\delta\varphi_\pm$ along GLs to the following equations:[19]

$$\frac{d^2\delta\varphi_+}{dx^2} + \frac{\omega(\omega + i\nu)}{s^2}(\delta\varphi_+ - \delta\varphi_-) = -\delta j\,(\nu - i\omega)\frac{4\pi d}{ks^2}, \tag{8}$$

$$\frac{d^2\delta\varphi_-}{dx^2} + \frac{\omega(\omega + i\nu)}{s^2}(\delta\varphi_- - \delta\varphi_+) = \delta j\,(\nu - i\omega)\frac{4\pi d}{ks^2}. \tag{9}$$

Here, ν is the collision frequency of electrons and holes in GLs with impurities and acoustic phonons and s is the characteristic velocity of plasma waves in GLs. The terms in the right-hand sides of Eqs. (8) and (9) are associated with the ac inter-GL current. The plasma wave velocity s is determined

by the net dc electron and hole density (i.e., by the Fermi energy) $\Sigma_0 \simeq (\mu_0/\hbar v_W)^2/\pi$ and the gate layer thickness d. In particular, $s \propto \Sigma_0^{1/4} d^{1/2} \propto V_0^{1/4} d^{1/4}$. As shown previously,[5,7] $s > v_W$ even at rather thin gate layers; s tends to v_W when d tends to zero. So that, in the case of thin gate layers under consideration, $s \gtrsim 10^8$ cm/s. In infinite (in the x-direction) double-GL structures, Eq. (8) governs the syn-phase plasma waves $\delta\varphi_+ = -\delta_- \propto \exp[i(qx - \omega t)]$ with the dispersion relation $\omega = s^* q$. Here the actual phase velocity $s* = s/\sqrt{2}$ differs[26,27] from the plasma-wave velocity in a two-dimensional structure with highly conducting (metal) gate,[13] which is equal to s. This distinction is due to the equality of the GL properties. However, in the double-GL structures with finite length of GL under consideration, the plasma waves are standing with the quantized wave numbers $q = q_n$ and, hence, the plasma frequencies $\omega = \omega_n = s^* q_n$, where $n = 0, 1, 2,\ldots$ is the index of the standing syn-phase plasma wave. Since the regions in which GLs do not overlap each other, i.e., the regions between the isolated (disconnected) edges of GLs and the contacts can contribute to the net capacitance of the double-GL structure under consideration (see Fig. 1, upper panel). However, the effect of these regions on the plasma oscillations is weak if the length, L_c, of these sections isolating GLs from the pertinent side contacts is not too long $L_c < L^2/d$.[16] Hence, considering just such a case, one can disregard the capacitance of these sections. This implies that one can use the following boundary conditions for Eqs. (8) and (9):

$$\delta\varphi_+\big|_{x=L} = \frac{\delta\varphi_A}{2}, \qquad \delta\varphi_-\big|_{x=-L} = -\frac{\delta\varphi_A}{2}, \qquad \frac{d\delta\varphi_+}{dx}\bigg|_{x=-L} = 0, \qquad \frac{d\delta\varphi|_-}{dx}\bigg|_{x=L} = 0, \tag{10}$$

where $\delta\varphi_A$ is the drop of the ac potential across the antenna, which is proportional to its radiation resistance r_A and the terminal ac current δJ, and $2L$ is the size of GLs [see Fig. 1(a)]. The latter boundary conditions reflect the fact that the displacement current between the disconnected edges and the contacts are negligible, and, therefore, the electron and hole currents are equal to zero at disconnected edges of GLs (at $x = -L$ in the upper GL and at $x = L$ in the lower GL). Considering that the net terminal ac current comprises the current created by a portion of the photogenerated carriers escaped from one GL and collected by another and the displacement current, one obtains

$$\delta J = 2LH\delta j - i\frac{\omega\, kH}{4\pi\, d}\int_{-L}^{L} dx(\delta\varphi_+ - \delta\varphi_-), \tag{11}$$

where H is the GL transverse size ($2LH$ is the GL area).

$$\delta\varphi_+ + \delta\varphi_- = Ax, \tag{12}$$

where A is a constant. Considering Eq. (12), Eqs. (8) and (9) can be presented as

$$\frac{d^2\delta\varphi_+}{dx^2} + \frac{2\omega(\omega + i\nu)}{s^2}\left(\delta\varphi_+ - \frac{A}{2}x - i\delta j\frac{2\pi\, d}{k\omega}\right) = 0, \tag{13}$$

$$\frac{d^2\delta\varphi_-}{dx^2} + \frac{2\omega(\omega + i\nu)}{s^2}\left(\delta\varphi_- - \frac{A}{2}x + \delta j\frac{2\pi\, d}{k\omega}\right) = 0. \tag{14}$$

Solving Eqs. (13) and (14) with boundary conditions (9), we obtain

$$A = -\frac{\delta\varphi_A + i\delta j\dfrac{2\pi d}{k\omega}}{L\left(\dfrac{\cos\gamma L}{\gamma L\sin\gamma L} - 1\right)}, \tag{15}$$

$$\delta\varphi_+ = \left(\frac{\delta\varphi_A}{2} + i\delta j\frac{2\pi d}{k\omega}\right)\left(\frac{\dfrac{\cos\gamma x}{\gamma L\sin\gamma L} - \dfrac{x}{L}}{\dfrac{\cos\gamma L}{\gamma L\sin\gamma L} - 1}\right) - i\delta j\frac{2\pi d}{k\omega}, \tag{16}$$

$$\delta\varphi_- = -\left(\frac{\delta\varphi_A}{2} + i\delta j\frac{2\pi d}{k\omega}\right)\left(\frac{\dfrac{\cos\gamma x}{\gamma L\sin\gamma L} + \dfrac{x}{L}}{\dfrac{\cos\gamma L}{\gamma L\sin\gamma L} - 1}\right) + i\delta j\frac{2\pi d}{k\omega}. \tag{17}$$

Here $\gamma = \sqrt{2\omega(\omega + i\nu)}/s$. Introducing the characteristic plasma frequency $\omega_p = \pi s/2\sqrt{2}L$, one obtains $\gamma L = \pi\sqrt{\omega(\omega + i\nu)}/2\omega_p$.

IV. PHOTOCURRENT AND OUTPUT THz POWER

From Eqs. (7), (11), (13), and (14), we obtain the following formula for the net terminal ac current:

$$\delta J = 2LH\frac{\left(\delta j - i\dfrac{\omega\, k}{4\pi\, d}\delta\varphi_A\right)}{\gamma(\cot\gamma L - \gamma L)}, \tag{18}$$

$$\delta\varphi_A = -\delta J\, r_A, \tag{19}$$

where r_A is the radiation resistance of the antenna. Excluding $\delta\varphi_A$ from Eqs. (16) and (17), we arrive at

$$\delta J = \frac{2LH\,\delta j}{\gamma(\cot\gamma L - \gamma L) - i\omega\, Cr_A} = \frac{R_0\,\delta P_\Omega}{\gamma(\cot\gamma L - \gamma L) - i\omega\tau_A}, \tag{20}$$

where $\delta P_\Omega = 2LH\hbar\Omega\,\delta I$, $C = kLH/2\pi\, d$ is the geometrical capacitance of the double-GL structure and $\tau_A = Cr_A$ is the characteristic recharging time.

Accounting for Eq. (20), for the emitted THz power, δP_ω we obtain

$$\delta P_\omega = \frac{\delta P_0}{|1 - i\omega\tau_e|^2|\gamma L(\cot\gamma L - \gamma L) - i\omega\tau_A|^2} \tag{21}$$

or

$$\delta P_\omega = \frac{\delta P_0}{(1 + \omega^2\tau_e^2)}\left|\left[\frac{\pi\sqrt{\omega(\omega + i\nu)}}{2\omega_p}\right]\left\{\cot\left[\frac{\pi\sqrt{\omega(\omega + i\nu)}}{2\omega_p}\right] - \left[\frac{\pi\sqrt{\omega(\omega + i\nu)}}{2\omega_p}\right]\right\} - i\omega\tau_A\right|^{-2}. \tag{22}$$

Here

$$\delta P_0 = \frac{1}{2} r_A R_0^2 \, \delta P_\Omega^2. \tag{23}$$

At $\omega \ll \tau_M^{-1}, \tau_A^{-1}, \tau_e^{-1}, \nu$, Eqs. (21) and (22) yield

$$\delta P_\omega = \frac{\delta P_0}{(1+\omega^2\tau_e^2)[1+\omega^2(\tau_M+\tau_A)^2]} \simeq \delta P_0. \tag{24}$$

Here $\tau_M = \pi^2\nu/4\omega_p^2$ is the Maxwell relaxation time in GLs, which is proportional to the double-GL structure capacitance and the GL resistance. If $\tau_M^{-1}, \tau_A^{-1}, \tau_e^{-1} < \omega < \nu$, Eq. (21) yields $\delta P_\omega \propto \omega^{-4}$.

However, in the devices with relatively low collision frequency, $\nu \ll \omega_p$, δP_ω can exhibit a steep rise when ω approaches to the plasma resonance frequencies, $\omega_n \propto \omega_p$.

Figures 3 and 4 show the frequency dependence of the normalized output power $\delta P_\omega/\delta P_0$ calculated using Eqs. (21) and (22) for different values of the collision frequency ν and L/s, i.e., for different values of the characteristic plasma frequency, $\omega_p = \pi s/2\sqrt{2}L$. The quantity $L/s \propto L/\Sigma_0^{1/4} d^{1/2} \propto L/V_0^{1/4} d^{1/4}$ is the main parameter characterizing the structure under consideration at given bias voltage. In Figs. 3 and 4, we assumed that $L/s = 0.25$–0.1 ps. This corresponds to the characteristic plasma frequencies $\omega_p/2\pi \simeq 0.7 - 1.77$ THz. We also set $\tau_e = 0.1$ ps, (for instance, $\tau_{relax} = 0.2$ ps and $w_{esc} = 0.5$) and $\tau_A = 0.1$ ps. If the inter-GL spacing $d = 10$ nm, $\omega_p/2\pi \simeq 0.7$ THz is achieved, for instance, when $2L \simeq 1875$ nm and $s = 3.75 \times 10^8$ cm/s (this corresponds to $\Sigma_0 \simeq 0.81 \times 10^{12}$ cm^{-2} and $\mu_0 = 100$ meV), whereas $\omega_p/2\pi \simeq 0.7$ THz is achieved, say, when $2L \simeq 1060$ nm and $s = 5.29 \times 10^8$ cm/s (this corresponds to $\Sigma_0 \simeq 3.26 \times 10^{12}$ cm^{-2} and $\mu_0 = 200$ meV).

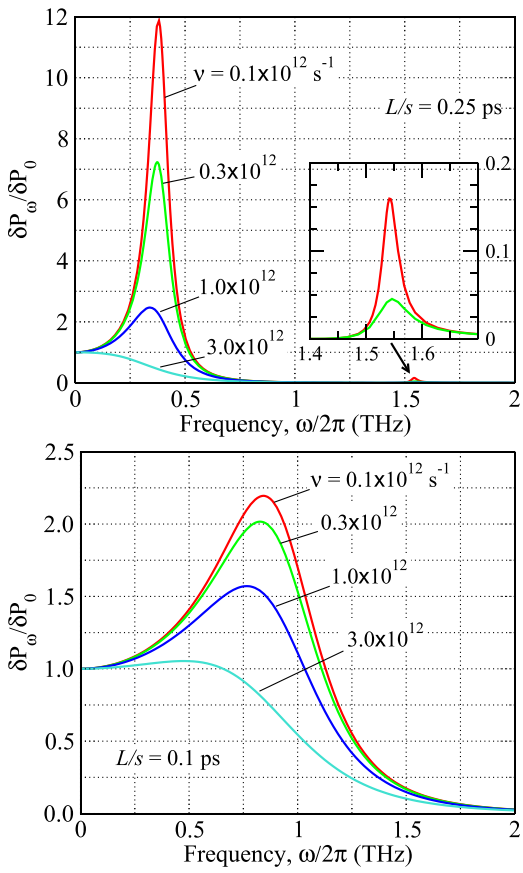

FIG. 3. Normalized output power $\delta P_\omega/\delta P_0$ versus frequency for different values of electron and hole collision frequency ν and for $L/s = 0.25$ ps, i.e., $\omega_p/2\pi \simeq 0.7$ THz (upper panel) and for $L/s = 0.1$ ps, i.e., $\omega_p/2\pi \simeq 1.77$ THz (lower panel). Inset on the upper panel shows the peaks corresponding to the first resonant frequency ($n = 1$) for $\nu = 0.1 \times 10^{12}$ s^{-1} and $\nu = 0.3 \times 10^{12}$ s^{-1}.

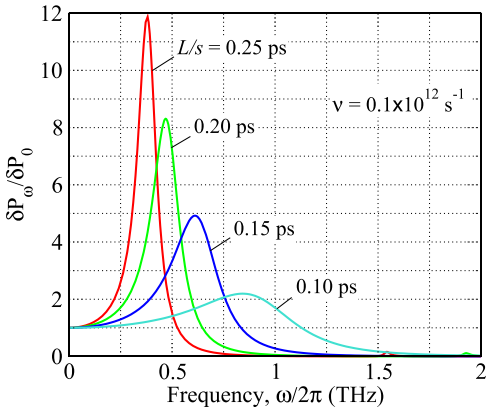

FIG. 4. Normalized output power $\delta P_\omega/\delta P_0$ versus frequency for different values of parameters L/s corresponding the plasma frequency $\omega_p \propto s/L$ in the range $\omega_p/2\pi \simeq 0.77 - 1.77$ THz.

As follows from Fig. 3, the output power exhibits the resonant behavior. The position of the resonant peaks and their height are determined by the plasma frequency ω_p and the collision frequency ν. An increase in ω_p leads to a shift in the peak position toward higher frequencies (compare the upper and lower panels in Fig. 3). Such a shift can be realized by varying the applied voltage V_0 (since $\omega_p \propto s/L \propto V_0^{1/4}$). The shift of the resonant peak with increasing plasma frequency, i.e., decreasing ratio L/s is readily seen in Fig. 4. As seen from Fig. 3, the peak height markedly increases and its width decreases with the decreasing collision frequency ν, i.e., with the increasing quality factor of the plasma resonances.

The resonant frequencies are $\omega_n = s^* q_n$. Here the wave numbers q_n determined by the quantization rule corresponding to the boundary conditions (10) are given by the following formulas: $q_0 = 0.86/L$, so that $f_0 = \omega_0/2\pi = 0.86\omega_p/\pi^2$ for the fundamental (zeroth) resonance and $q_n = \pi(n + 1/\pi^2 n)/L$ and hence $f_n = (2\omega_p/\pi)(n + 1/\pi^2 n)$ for higher resonances. However, for the chosen parameters, only the zeroth resonant peaks are substantially pronounced. They correspond to $f_0 \simeq 0.38$ THz and $f_0 \lesssim 1$ THz. A relatively low peak, which corresponds to the first resonance (n = 1), can be detected at $f_1 \simeq 1.52$ THz as seen in the upper panel of Fig. 3. Relatively low values of the responsivity and, hence, of the output power at higher resonances is associated with quasi-periodical spatial distributions of the ac potential along GL. Due to this factor, the displacement inter-GL current in different parts of the structure has the opposite sign. However, even this weak resonance can lead to a marked output power in the THz range: $\delta P_\omega/\delta P_0 \simeq 15\%$ (see the inset in Fig. 3, upper panel).

V. COMMENTS

For $\hbar\Omega \simeq 1$ eV and $w_{esc} \lesssim 1$, we obtain $R_0 \simeq 0.023$ A/W. This value of the low-frequency responsivity is of the same

order of magnitude as in UTC-PDs[22,23] with relatively thick (typical) absorption layer ($W \simeq 100$ nm), which corresponds to somewhat long electron transit time across this layer in UTC-PDs. This implies that the output THz power, δP_0, at the low end of the THz range of DG-PMs and UTC-PDs is of the same order of magnitude. In particular, at $\delta P_\Omega \simeq 1$ W, one obtains $2LH\delta j \simeq 15 - 30$ mA. Assuming $r_A = 1\,\Omega$ (as follows from Refs. 22 and 23), for a DG-PM with the same antenna as in UTC-PDs we obtain $\delta P_0 \simeq 225 - 900$ μW.

The roll-off of the output power in DG-PTs with increasing difference frequencies ω (i.e., the frequency of output radiation) can be markedly slower than that in UTC-PDs because of a shorter escape time τ_{esc} and shorter transit time τ_{tr}. The point is that in UTC-PDs, the escape time is determined by the transit time of the photoexcited electrons across the absorption layer due their diffusion and drift. However, a decrease in the thickness of the absorption layer leads to a decrease in the quantum efficiency and, consequently, in the responsivity, so that the possibility of the narrowing of the absorption layer in UTC-PDs is limited.

At relatively high frequencies ω (in the THz range), the conditions of plasma resonances can be fulfilled, and the resonant peaks of the ac photocurrent δJ and the output power can be fairly high, providing the sufficient quality of GL and properly chosen antenna parameters (or special structure for the THz radiation output). Figure 5 shows the transformation of the frequency dependence of the output power with the varying recharging time $\tau_A \propto \tau_A$. As follows from Eqs. (21)–(23) and from Fig. 5, a decrease in the antenna radiation resistance leads to a decrease in the output power at low frequencies and its rise at the resonance.

However, at higher frequencies, at which the UTC-PD output power dramatically falls with increasing frequency, DG-PMs can provide markedly higher output THz power due to short transit times and the resonant excitation of plasma oscillations. Indeed, as seen from Fig. 3, the output power in the DG-PM based on the double-GL structures with the realistic quality of GL (realistic values of the collision frequency ν) at the fundamental plasma resonance can markedly exceed its value at low frequencies. The main factors limiting the height of the resonant peaks are the value of collision frequency ν (plasma resonance quality factor) and the recharging time τ_A, associated with the double-GL structure geometrical capacitance and the antenna radiation resistance. At $2LH = 10$ μm^2, $d = 10$ nm, $k = 10$, and $r_A = 1 - 10\,\Omega$, one obtains $\tau_A \simeq (0.03 - -0.3)$ ps, so that at $\omega/2\pi = 1$ THz, the product $\omega\tau_A \simeq 0.188 - 1.88$.

The most crucial requirement to realize effective DG-PMs is the achievement of the probability of the escape of photoexcited electrons $w_{esc} \sim 1$. This enables to use either the double-GL structures with sufficiently low inter-GL barrier [to satisfy inequality (1) at reasonable energies of optical photons $\hbar\Omega$] or the structures with a thin tunnel transparent barrier.

The quantum efficiency and, hence, the output THz power can be markedly increased using several stacked double-GL structures or double-GL structures integrated with optical wave guides and the lateral input of modulated optical radiation (see Fig. 1, lower panels).

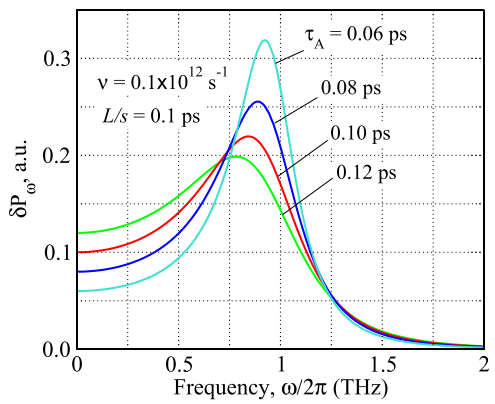

FIG. 5. Frequency dependences of output power δP_ω for different values of recharging time τ_A. The chosen value of parameter L/s at $d = 10$ nmc and $2L = 1060$ nm corresponds to electron and hole densities $\Sigma_0 \simeq 3.26 \times 10^{12}$ cm^{-2}.

VI. CONCLUSIONS

In summary, we proposed THz photomixers based on double-GL structures (DG-PMs), which exploit the absorption of radiation of two lasers with the photon frequencies close to each other or by ultra-short optical pulses. The photomixing mechanism involves the photoexcitation of electrons, their transfer between GL due to thermionic or tunneling processes, and the excitation of plasma oscillations the syn-phase variations of the electron and hole densities. We developed the DG-PM device model, which accounts for the processes mentioned above. Calculated the DG-PM characteristics, in particular, the frequency dependence of the output power from low to THz frequencies for different parameters of GL-structures. The model predicts that the radiation output power can exhibit sharp plasma resonant peaks in the THz range with the peak power markedly exceeding that at relatively low frequencies. Due to a relatively high quantum efficiency of optical absorption in GLs, short transit time, and the possibility of the resonant plasma oscillation excitation, DG-PMs can surpass the photomixers based on the standard heterostructures, in particular those based on UTC-PDs.

ACKNOWLEDGMENTS

This work was supported by the Japan Society for Promotion of Science, Grant-in-Aid for Specially Promoted Research (23000008), Japan, and PIRE TeraNano Program, NSF, USA. The work at RPI was supported by the Army Research Laboratory under ARL MSME Alliance.

[1]R. R. Nair, P. Blake, A. N. Grigorenko, K. S. Novoselov, T. J. Booth, T. Stauber, N. M. R. Peres, and A. K. Geim, Science **320**, 1308 (2008).
[2]J. M. Dawlaty, S. Shivaraman, J. Strait, P. George, M. Chandrashekhar, F. Rana, M. G. Spencer, D. Veksler, and Y. Chen, Appl. Phys. Lett. **93**, 131905 (2008).
[3]F. Bonnaccorso, Z. Sun, T. Hasan, and A. C. Ferrari, Nature Photon. **4**, 611 (2010).
[4]A. H. Castro Neto, F. Guinea, N. M. R. Peres, K. S. Novoselov, and A. K. Geim, Rev. Mod. Phys. **81**, 109 (2009).
[5]V. Ryzhii, Jpn. J. Appl. Phys. **45**, L923 (2006).
[6]O. Vafek, Phys. Rev. Lett. **97**, 266406 (2006).
[7]V. Ryzhii, A.Satou, and T. Otsuji, J. Appl. Phys. **101**, 024509 (2007).

[8]L. A. Falkovsky and A. A. Varlamov, Eur. Phys. J. B **56**, 281 (2007).
[9]E. H. Hwang and S. Das Sarma. Phys. Rev. B **80**, 205405 (2009).
[10]D. Svintsov, V. Vyurkov, S. Yurchenko, T. Otsuji, and V. Ryzhii, J. Appl. Phys. **111**, 083715 (2012).
[11]G. W. Hanson, J. Appl. Phys. **103**, 064302 (2008).
[12]A. A. Dubinov, V. Ya. Aleshkin, V. Mitin, T. Otsuji, and V. Ryzhii, J. Phys. Condens. Mater. **23**, 145302 (2011).
[13]M. Dyakonov and M. Shur, IEEE Trans. Electron Devices **43**, 1640 (1996).
[14]J. Lusakowski, W. Knap, N. Dyakonova, L. Varani, J. Mateos, T. Gonzales, Y. Roelens, S. Bullaert, A. Cappy, and K. Karpierz, J. Appl. Phys. **97**, 064307 (2005).
[15]F. Teppe, W. Knap, D. Veksler, M. S. Shur, A. P. Dmitriev, V. Yu. Kacharovskii, and S. Rumyantsev, Appl. Phys. Lett. **87**, 052107 (2005).
[16]V. Ryzhii, A. Satou, W. Knap, and M. S. Shur, J. Appl. Phys. **99**, 084507 (2006).
[17]A. El Fatimy, F. Teppe, N. Dyakonova, W. Knap, D. Seliuta, G. Valusis, A. Shcherepetov, Y. Roelens, S. Bollaert, A. Cappy, and S. Rumyantsev, Appl. Phys. Lett. **89**, 131926 (2006).
[18]J. Torres, P. Nouvel, A. Akwaoue-Ondo, L. Chusseau, F. Teppe, A. Shcherepetov, and S. Bollaert, Appl. Phys. Lett. **89**, 201101 (2006).
[19]V. Ryzhii, I. Khmyrova, A. Satou, P. O. Vaccaro, T. Aida, and M. S. Shur, J. Appl. Phys. **92**, 5756 (2002).
[20]A. Satou, V. Ryzhii, I. Khmyrova, M. Ryzhii, and M. S. Shur, J. Appl. Phys. **95**, 2084 (2004).
[21]T. Otsuji, M. Hanabe and O. Ogawara, Appl. Phys. Lett. **85**, 2119 (2004).
[22]M. Liu, X. Yin, E. Ulin-Avila, B. Geng, T. Zentgraf, L. Ju, F. Wang, and X. Zhang, Nature **474**, 64 (2011).
[23]L. Britnel, R. V. Gorbachev, R. Jalil, B. D. Belle, F.Shedin, A. Mishenko, T. Georgiou, M. I. Katsnelson, L. Eaves, S. V. Morozov, N. M. R. Peres, J. Leist, A. K. Geim, K. S. Novoselov, and L. A. Ponomarenko, Science **335**, 947 (2012).
[24]M. Liu, X. Yin, and X. Zhang, Nano Lett. **12**, 1482 (2012).
[25]T. Georgiou, R. Jalil, B. D. Bellee, L. Britnell, R. V. Gorbachev, S. V. Morozov, Y.-J. Kim, A. Cholinia, S. J. Haigh, O. Makarovsky, L. Eaves, L. A. Ponimarenko, A. K. Geim, K. S. Nonoselov, and A. Mishchenko, Nature Nanotechnol. **8**, 100–103 (2013).
[26]V. Ryzhii, T. Otsuji, M. Ryzhii, and M. S. Shur, J. Phys. D: Appl. Phys. **45**, 302001 (2012).
[27]V. Ryzhii, T. Otsuji, M. Ryzhii, V. G. Leiman, S. O. Yurchenko, V. Mitin, and M. S. Shur, J. Appl. Phys. **112**, 104507 (2012).
[28]T. Stauber and G. Gomez-Santos, Phys. Rev. B **85**, 075410 (2012).
[29]J.-J. Zhu, S. M. Badalyan, and F. M. Peters, Phys. Rev. B **87**, 085401 (2013).
[30]D. Svintsov, V. Vyurkov, V. Ryzhii, and T. Otsuji, J. Appl. Phys. **113**, 053701 (2013).
[31]S. M. Duffy, S. Verhese, K. A. McIntoshy, A. Jackson, A. C. Gossard, and S. Matsuura, IEEE Trans. Microwave Theory Tech. **49**, 1032 (2001).
[32]A. Stohr, A. Malcoci, A. Sauerwald, I. C. Mayorga, R. Gusten, and D. Jager, IEEE J. Lightwave Technol. **21**, 3962 (2003).
[33]H. Ito, S. Kodama, Y. Muramoto, T. Furuta, T. Nagatsuma, and T. Ishibashi, IEEE Sel. Topics Quantum Electron. **10**, 709 (2004).
[34]H. Ito, F. Nakajima, T. Furuta, and T. Ishibashi, Semicond. Sci. Technol. **20**, S191 (2005).
[35]V. Ryzhii, I. Khmyrova, M.Ryzhii, A. Satou, T. Otsuji, V. Mitin, and M. S. Shur, Int. J. High Speed Electron. Syst. **17**, 521 (2007).